ELSEVIER

European Journal of Radiology 65 (2008) 15–28

EJR
EUROPEAN JOURNAL OF RADIOLOGY

www.elsevier.com/locate/ejrad

Review

Cardiac MRI of ischemic heart disease at 3 T: Potential and challenges

Oliver Wieben [a,b,*], Christopher Francois [a,1], Scott B. Reeder [a,b,c,d,2]

[a] *Department of Radiology, University of Wisconsin, Madison, WI 53792-3252, United States*
[b] *Department of Medical Physics, University of Wisconsin, Madison, WI 53792-3252, United States*
[c] *Department of Biomedical Engineering, University of Wisconsin, Madison, WI 53792-3252, United States*
[d] *Department of Medicine, University of Wisconsin, Madison, WI 53792-3252, United States*

Received 30 October 2007; accepted 30 October 2007

Abstract

Cardiac MRI has become a routinely used imaging modality in the diagnosis of cardiovascular disease and is considered the clinically accepted gold standard modality for the assessment of cardiac function and myocardial viability. In recent years, commercially available clinical scanners with a higher magnetic field strength (3.0 T) and dedicated multi-element coils have become available. The superior signal-to-noise ratio (SNR) of these systems has lead to their rapid acceptance in cranial and musculoskeletal MRI while the adoption of 3.0 T for cardiovascular imaging has been somewhat slower. This review article describes the benefits and pitfalls of magnetic resonance imaging of ischemic heart disease at higher field strengths. The fundamental changes in parameters such as SNR, transversal and longitudinal relaxation times, susceptibility artifacts, RF (B_1) inhomogeneity, and specific absorption rate are discussed. We also review approaches to avoid compromised image quality such as banding artifacts and inconsistent or suboptimal flip angles. Imaging sequences for the assessment of cardiac function with CINE balanced SSFP imaging and MR tagging, myocardial perfusion, and delayed enhancement and their adjustments for higher field imaging are explained in detail along with several clinical examples. We also explore the use of parallel imaging at 3.0 T to improve cardiac imaging by trading the SNR gain for higher field strengths for acquisition speed with increased coverage or improved spatial and temporal resolution. This approach is particularly useful for dynamic applications that are usually limited to the duration of a single breath-hold.

Keywords: Cardiac imaging; Magnetic resonance imaging; Cardiac function; 3.0 T; Cardiac perfusion; Viability imaging; Steady-state free precession

Contents

1. Introduction 16
2. General considerations 16
   2.1. SNR 16
   2.2. Relaxation times 16
   2.3. Chemical shift and susceptibility 16
   2.4. Specific absorption rate (SAR) 17
   2.5. Dielectric effects—B_1 inhomogeneity 17
   2.6. Parallel imaging 18
3. Assessment of cardiac function with gradient echo sequences 18
   3.1. Gradient echo sequences 18
   3.2. bSSFP imaging at 3.0 T 19

* Corresponding author at: University of Wisconsin – Madison, Departments of Medical Physics and Radiology, J5/150 Clinical Science Center, 600 Highland Avenue, Madison, WI 53792-3252, United States. Tel.: +1 608 263 0793; fax: +1 608 265 9840.
E-mail addresses: owieben@wisc.edu (O. Wieben), cfrancois@uwhealth.org (C. Francois), sreeder@wisc.edu (S.B. Reeder).
[1] Present address: University of Wisconsin – Madison, Departments of Medical Physics and Radiology, Box 3252 Clinical Science Center-E3, 600 Highland Ave, Madison, WI 53792, USA. Tel.: +1 608 263 1198.
[2] Present address: University of Wisconsin – Madison, Department of Radiology, Medical Physics, Biomedical Engineering, and Medicine, 600 Highland Ave, E1/374, Madison, WI 53792, USA. Tel.: +1 608 265 9964.

0720-048X/$ – see front matter © 2007 Elsevier Ireland Ltd. All rights reserved.
doi:10.1016/j.ejrad.2007.10.022

3.3. India-Ink artifact with bSSFP 21
4. MR tagging 22
5. First pass perfusion imaging 22
6. Viability imaging—delayed enhancement 25
7. Conclusion 26
References 26

1. Introduction

Each year, 1.2 million cases of coronary heart disease (CHD) are reported in the US alone, one-third of whom die of the disease. While the death rate of CHD has dramatically decreased over the past 30 years, CHD still accounts for almost 20% of all deaths in the US [1]. Improved diagnosis and the advent of statin pharmaceuticals [2] has led to continued improvement in patient outcomes. Many of these patients undergo catheterizations and in approximately 20% of the subjects no disease is detected. In another 30% of the patients, disease is detected but no intervention is performed while the remaining 50% undergo therapy in form of invasive coronary angiography (angioplasty and stenting) or coronary artery bypass (CABG). Cardiac magnetic resonance imaging (CMR) has become a routinely used modality for the diagnosis of ischemic heart disease and can provide non-invasive evaluation of reperfusion therapy through comprehensive evaluation of wall motion, global function, perfusion and viability [3]. In fact, CMR is widely considered the clinical gold standard for viability imaging by providing high resolution images of post-contrast gadolinium enhanced acquisitions that accurately depict the transmurality of myocardial infarction, which is critical to guide revascularization therapy [4].

Technical advances that improve the ability of MRI to visualize pathological changes in the heart with improved spatial and/or temporal resolution can only improve the diagnostic capabilities of this modality for the diagnosis and characterization of ischemic heart disease. Clinical 3.0 T scanners are increasingly available and are capable of performing high quality CMR. Increases in signal-to-noise (SNR) performance and changes in NMR relaxation parameters (T_1, T_2) offer tremendous potential to "push the envelope", advancing the ability of CMR to diagnose ischemic heart disease. However, cardiac imaging at a higher field strength also poses additional challenges that include increased radiofrequency (RF) induced energy deposition, higher demands on the shimming to compensate for amplified susceptibility artifacts and increased B_1 field inhomogeneities. It is the purpose of this review article to explore the potential of cardiac imaging at 3.0 T, as well as the challenges of high field imaging that must be addressed.

2. General considerations

2.1. SNR

One of the most appealing promises of imaging at a higher field strength is the increase in signal-to-noise ratio (SNR). In current MR scanners, the noise in most imaging applications is dominated by the intrinsic noise caused by random motion of electrons in the patient's tissue while electrical noise from the receiving circuit and other external noise contributions are usually negligible. At field strengths larger then 1.0 T, the MR signal exhibits quadratic growth with the field strength B_0 while the noise has a linear B_0 dependence [5]. Therefore, one would expect a gain of two in SNR when increasing the main magnetic field from 1.5 T to 3.0 T, with all other factors being equal [6]. However, the resulting signal, contrast, and image quality are heavily influenced by several other parameters that are affected by the change in field strength. These include the longitudinal and transversal relaxation times (T_1 and T_2) of the tissues, artifacts from off-resonances and B_1 field inhomogeneities, RF coil design, and pulse sequence adjustments that may be required due to safety constraints regarding the allowable energy deposited into the body from the RF pulses.

2.2. Relaxation times

With an increase in the field strength from 1.5 T to 3.0 T, the transverse relaxation time T_2 in most tissues experiences only a small decrease. The longitudinal relaxation time T_1, however, has been reported to increase with the third root of the field strength [7]. Values for T_1 and T_2 of tissues relevant for cardiac imaging reported in the literature [7–13] are summarized in Table 1. While these values vary across the studies, the reported trends are similar: the T_2 decreases slightly while the T_1 increases by larger amounts. The differences in the reported values are most likely due to differences in the measurement techniques, the tissue sources, and other factors. For example, Stanisz et al. [12] used tissue samples from mice and human blood for in-vitro measurements with high precision, Sharma et al. [13] analyzed 10 volunteers, Bi et al. [11] and Schaer et al. [10] extrapolated data from prior studies across a wide magnetic field range [7], and the measurements from Noeske et al. [9] were obtained from a single volunteer over a limited range of inversion times.

The relaxation rates R_1 and R_2 of gadolinium based contrast agents have been reported to decrease with an increase in field strength [14,15]. While the changes in relaxivity somewhat reduce the T_1 shortening caused by the contrast agent, the effect is rather small and has not been an issue in our experience.

2.3. Chemical shift and susceptibility

The precession frequency, also referred to as the Larmor frequency, is linearly dependent on the magnetic field strength.

Table 1
T_1 and T_2 values of oxygenated blood and normal myocardium at 1.5 T and 3.0 T as reported in the literature

Parameter	Bi et al. [11] and Schar et al. [10]	Noeske et al. [9]	Sharma et al. [13]	Stanisz et al. [12]	Stanisz et al. [8]
Measurement method	Analytically derived from [7]	In-vivo measurements from 1 volunteer	In-vivo measurements from 10 volunteers	In-vitro measurements from mouse heart and human blood	In vitro measurement of human blood
Oxygenated blood – T_1 at 1.5 T	1200 ms		1580 ms	1441 ± 120 ms	
Oxygenated blood – T_2 at 1.5 T	200 ms			290 ± 30 ms	327 ± 40 ms
Normal myocardium – T_1 at 1.5 T	867 ms		1070 ms	1030 ± 34 ms	
Normal myocardium – T_2 at 1.5 T	57 ms			40 ± 6 ms	
Oxygenated blood – T_1 at 3.0 T	1512 ms	1550 ± 85 ms	1690 ms	1932 ± 85 ms	
Oxygenated blood – T_2 at 3.0 T	141 ms			275 ± 50 ms	
Normal myocardium – T_1 at 3.0 T	1115 ms	1115 ± 10 ms	1200 ms	1471 ± 31 ms	
Normal myocardium – T_2 at 3.0 T	41 ms			47 ± 11 ms	

For protons, the precession frequency increases from 63.9 MHz to 127.8 MHz when the field strength increases from 1.5 T to 3.0 T. Such an increase in field strength also leads to a wider separation of metabolites in their respective precession frequencies. For example, the resonance frequency of protons in fat precesses 210 Hz slower than free protons at 1.5 T while this difference doubles to 420 Hz at 3.0 T. The increased chemical shift is highly beneficial for all MR spectroscopic applications including cardiac spectroscopy [16] but the effect also worsens chemical shift artifacts and amplifies off-resonances from susceptibility at tissue interfaces such as lung and tissue around the heart [17]. This can lead to signal loss in imaging pixels due to increased intravoxel dephasing. The decreased B_0 inhomogeneity also leads to banding artifacts when imaging with balanced steady-state free precession (bSSFP) sequences. As described below, the use of a scouting method to identify the optimal synthesizer frequency [18] or improved shimming over a localized field-of-view or with higher order shimming corrections [10] are used to minimize these artifacts in the regions of interest.

2.4. Specific absorption rate (SAR)

The use of an RF field, or B_1 field, to excite the magnetic spins also has the effect that energy is deposited into the imaged object. Patient safety guidelines by regulatory agencies dictate the thresholds for the specific absorption rate (SAR) allowed for human imaging in order to keep potential global and local rises in body temperature within an acceptable range. These SAR guidelines usually do not pose any limitations to imaging applications at 1.5 T. The flip angle α achieved with an RF pulse is proportional to the integral of the amplitude of the alternating field B_1 over the time it is applied:

$$\alpha \propto \int B_1 \, dt \approx B_1 \Delta T \tag{1}$$

In rapid imaging, high B_1 fields are used to minimize the pulse duration (ΔT) and, therefore, the repetition time and the echo time. However, the SAR is proportional to the integral of the square of amplitude of the alternating field B_1 over the time it is applied:

$$\text{SAR} \propto \int B_1^2 \, dt \approx B_1^2 \Delta T \tag{2}$$

Importantly, the B_1 amplitude required to achieve a given flip angle doubles at 3.0 T, Thus, for the same RF pulse design, the SAR increases by a *factor of four* at 3.0 T compared to 1.5 T. Therefore, sequences with rapidly repeated high flip angles require adjustments to maintain a safe SAR. This is most important for fast spin echo sequences, 3D gradient echo sequences with short repetition times, and, most relevant for the context of this review, balanced steady-state free precession (bSSFP) sequences that require ultrashort repetition times. Several methods can be used to partially overcome SAR limitations in these situations. (1) Reducing the flip angle is a straight-forward simple and effective way to reduce the SAR but this may lead to undesired alterations in tissue contrast. However, as we will show below, the effect on bSSFP sequences is relatively minor as the bSSFP contrast is not strongly dependent on flip angle. (2) Lengthening the total duration of the RF pulse reduces the SAR because the increase due to the longer pulse is more than offset by the reduction from the B_1 amplitude when maintaining the flip angle. (3) The use of parallel imaging techniques can reduce the total number of RF pulses required to complete the acquisition and, therefore, reduce the SAR. (4) The use of RF pulses that are designed to use B_1 amplitudes that stay more constant (VERSE – variable-rate selective excitation) rather than being defined by a major lobe with a high peak [19]. (5) Advanced flip angle modification schemes have been proposed to maintain similar contrast while reducing the average flip angle for fast spin echo sequences [20,21].

2.5. Dielectric effects—B_1 inhomogeneity

The frequency of the RF pulses used to modify the state of the magnetic spins in the tissues needs to match their precession frequency and their wavelength is inversely proportional to that frequency. The actual wavelength depends on the electrical permittivity of the medium that the RF wave is propagating in. At 3.0 T, the wavelength for proton imaging becomes smaller than the human body where the effective wavelength is smaller than

1 m inside the body [5]. This so-called "dielectric effect" leads to standing wave patterns and other effects can occur that cause an inhomogeneous B_1 field. Inhomogeneous B_1 fields result in non-uniform flip angles across imaging volume. Fortunately, the signal and contrast in bSSFP sequences are relatively insensitive to flip angle variations and, therefore, B_1 inhomogeneity is not a challenge for this pulse sequence. However, inversion recovery spoiled gradient echo sequences for delayed enhanced viability imaging require highly uniform inversion pulses to ensure robust inversion of magnetization across the heart. As described by Gutberlet [22], non-uniform inversion flip angle results in inadequate inversion leading to areas of poorly nulled myocardium. The use of adiabatic pulses can provide a more homogeneous flip angle as shown for viability imaging [22] or for coronary imaging with T_2 preparation [23].

2.6. Parallel imaging

Parallel MRI exploits the spatial sensitivities of multiple receiver coils in a phased array to reduce the required number of phase encoding steps [24–26]. In this way, image acquisitions achieve significant "reduction" factors, typically $R = 2$–6 with cardiac coils with up to 32 receiving elements [27–31], which permits tremendous improvements in spatial coverage for breath-hold imaging applications. The major trade-off with parallel imaging is a decrease in image SNR, i.e.:

$$SNR_R = \frac{SNR_o}{g\sqrt{R}}$$

where SNR_o is the SNR of an unaccelerated image, the $\sqrt{R}$ term reflects the drop in SNR from reduced scan time, and g, the "geometry factor", which is always one or greater, reflects the ill-conditioning of image unwrapping and is a measure of the performance of a coil and the parallel imaging algorithm. The g-factor increases at higher reduction factors, limiting practically achievable accelerations. Importantly, the performance of parallel imaging greatly improves at 3.0 T, resulting from the smaller wavelength of the RF signal. This improves the effective coil separation and maintains g close to one at higher acceleration factors [32,33].

At 3.0 T, parallel imaging provides the flexibility to trade this increase in SNR for tremendous reductions in scan time or greater coverage within the same breath-hold [34]. For example, with a reduction factor of 4, and assuming $g = 1$, we can achieve a four-fold increase in scan coverage in the same scan time, with the same SNR performance and image quality as 1.5 T. In reality, this tremendous improvement may be tempered by other factors discussed in this paper (T_1, SAR, B_1 inhomogeneities, etc.).

3. Assessment of cardiac function with gradient echo sequences

3.1. Gradient echo sequences

Cardiac MRI has become the gold standard of any imaging modality for the assessment of wall motion and function. CINE cardiac imaging of the beating heart is accomplished with rapid gradient echo sequences that can provide image series of high spatial and temporal resolution with good contrast between myocardium and blood. Whole heart coverage is usually achieved by imaging of one or several slices over multiple breath-holds to allow for the measurements of global functional parameters such as cardiac output, ejection fraction, ventricular mass, etc. In addition, these image series allow for the assessment of regional wall thickness and motion abnormalities throughout the cardiac cycle.

Initially, CINE cardiac imaging [35] was performed with spoiled gradient echo sequences, also known as fast low angle shot (FLASH) [36], spoiled gradient recalled acquisition in the steady-state (SPGR), or fast field echo (FFE), an acquisition technique that uses RF spoiling and gradient spoiling to achieve a steady-state condition for the longitudinal magnetization. In balanced SSFP (steady-state free precession) imaging, no spoiling is used and both the transverse and the longitudinal magnetizations reach a steady-state and contribute to the MR signal [37]. This approach, also known as true fast imaging with steady-state precession (trueFISP) [38], fast imaging employing steady-state acquisition (FIESTA), and balanced fast field echo (bFFE), has only recently become practical for clinical cardiac imaging [39] due to hardware improvements particularly in gradient performance and field shimming to avoid artifacts described below. Despite its recent introduction into cardiac imaging, bSSFP has rapidly become the gold standard for CINE cardiac imaging, as a result of its high SNR performance and excellent blood-myocardial contrast. While the image contrast in the rapid SPGR sequence depends mostly on T_1 dependent and inflow effects for a high blood signal, bSSFP provides an inherently high steady-state signal for species with a large T_2 over T_1 ratio, such as blood. Due to its short repetition time, high SNR efficiency, exquisite blood-myocardial contrast, and advantages for automated segmentation it has become the method of choice for cardiac CINE imaging at 1.5 T [40,41].

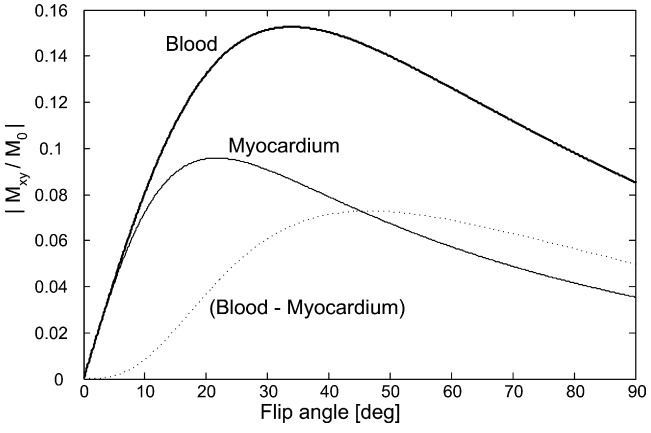

Fig. 1. Magnitude of the transverse magnetization for blood (solid line), myocardium (thin line), and their difference (dotted line) as a function of the flip angle for imaging with a bSSFP sequence at 3 T.

3.2. bSSFP imaging at 3.0 T

The gain in SNR with higher field strength is accompanied with several challenges and limitations for bSSFP imaging at 3.0 T including increased dark banding artifacts from off-resonances and suboptimal flip angle choices because of SAR restrictions. Fig. 1 shows simulation results for the bSSFP signal in blood and myocardium as a function of the flip angle. This simulation assumes steady-state conditions [42,43] with the following parameters: TR = 3.8 ms; TE = 1.9 ms; flip angle = 40°; T_1 = 1512 ms and T_2 = 141 ms for blood; and T_1 = 1115 ms and T_2 = 41 ms for the myocardium, similar to the parameters used by others [10,11].

The in-vivo signal behavior of the blood is likely somewhat different because of additional inflow effects that are not accounted for here, but this simulation demonstrates the large blood-myocardial signal contrast achievable with bSSFP imaging. Despite the challenges faced by bSSFP, the very large CNR and improvement in SNR is highly motivating to address these challenges rather than revert to using SPGR sequences at 3.0 T. For example, it can be shown that the bSSFP signal for normal myocardium is more than twice the signal from the spoiled gradient echo sequence for optimized flip angle choices. Importantly, Fig. 1 also demonstrates that the bSSFP contrast is relatively constant for flip angles exceeding 35°, with an optimal flip angle at 40–45° in order to maximize the contrast between blood and myocardium. Therefore, the bSSFP sequence is relatively robust in respect to B_1 inhomogeneities that cause inconsistent flip angles.

One limitation of using bSSFP sequences is their sensitivity to severe imaging artifacts for off-resonances due to a complex signal behavior. The magnitude and the phase of the bSSFP signal depends not only on the T_1 and T_2 of the imaged species and the TR and TE of the acquistion but also on the phase (β) that accumulates during a TR as a result of magnetic field inhomogeneities or chemical shift. The presence of magnetic field

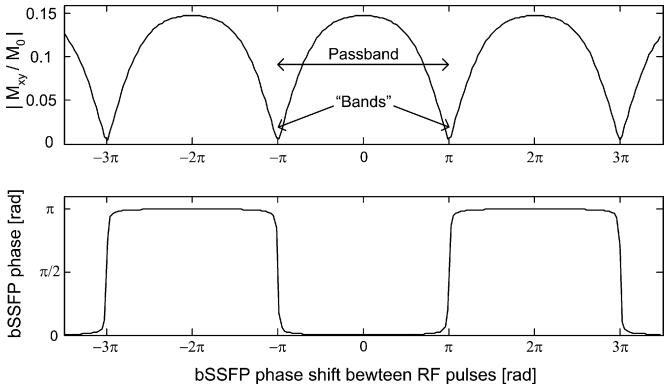

Fig. 2. Signal behavior in balanced SSFP imaging. The magnitude of the transversal magnetization (top row) and the phase (lower row) of the bSSFP signal are plotted as a function of β, the phase shift between RF pulses with representative parameters for imaging at 3.0 T: T_1 = 1512 ms and T_2 = 141 ms (blood), TR = 3.8 ms, TE = TR/2 = 1.9 ms, flip angle = 45°. The signal in the magnitude response drops significantly at voxels where the field inhomogeneity causes a 180° (π) phase shift between RF pulses ("bands").

inhomogeneities (ΔB_0) leads to a phase shift between each RF pulse,

$$\beta = \gamma \times \Delta B_0 \times \mathrm{TR} \quad [3],$$

where γ is the gyromagnetic ratio.

The magnitude and phase of the bSSFP signal as a function of β are shown in Fig. 2. An off-resonance phase of β = 180° (π radians) corresponds to an isochromat that is off-resonance by 1/(2 × TR) so that Fig. 2 can also be interpreted as a spectral response. At this phase offset, the signal in the magnitude response drops precipitously, corresponding to severe signal loss at locations in the image where the field inhomogeneity causes a 180° (π) phase shift between RF pulses. Since the off-resonances from susceptibilities are directly proportional to the field strength, bSSFP imaging at 3 T is equivalent to imaging at

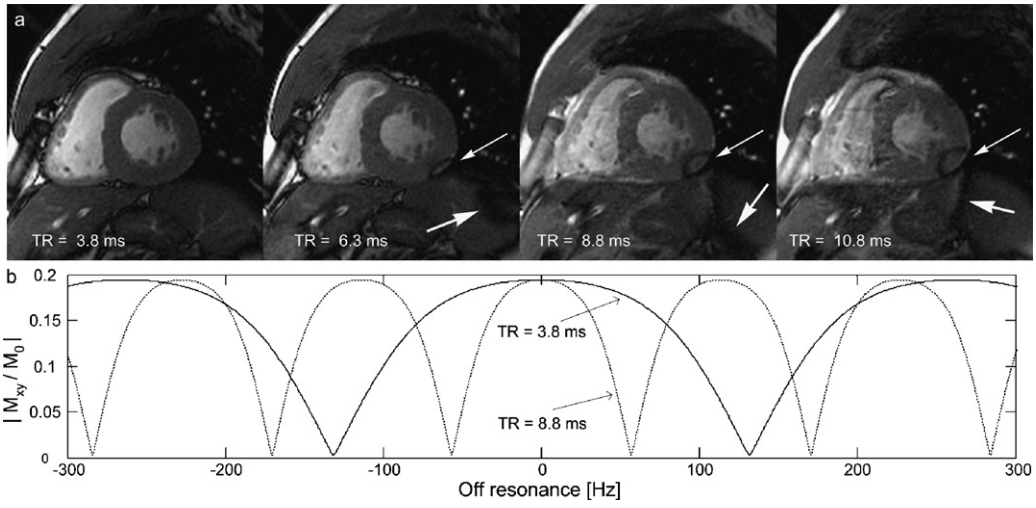

Fig. 3. Effect of changes in TR on the signal behavior in bSSFP imaging. The cine images acquired at 1.5 T (a) with longer TR suffer from banding artifacts, most notably in the ventricular wall (thin arrows). The passbands narrow for longer TRs and cause signal drops at lower off-resonances as shown in the magnitude plot of the steady-state magnetization based on typical acquisition parameters at 1.5 T (b) with the following parameters: T_1 = 1200 ms and T_2 = 200 ms (blood); TE = TR/2; flip angle = 45°; and TR = 3.8 ms (solid line) and 8.8 ms (dotted line).

1.5 T at twice the TR with respect to these "banding" artifacts.

There are two main strategies to reducing banding artifacts: reducing the TR, and reducing the field inhomogeneities over the heart. Fig. 3 demonstrates the significance of short repetition times at 1.5 T where a banding artifact (arrow) is apparent in the free myocardial wall for longer repetition times. As the TR is shortened, the band is pushed out of the myocardium and it completely disappears at a TR of 3.8 ms. The magnitude response in Fig. 3(b) shows that an image is free of banding artifacts for all voxels with off-resonances less than ±40 Hz when acquired with a TR of 8.8 ms. If the TR is reduced to 3.8 ms, the passband widens and voxels with up to ±100 Hz are properly represented without significant signal drops.

One effective strategy that we have used to reduce the TR of the bSSFP acquisition is the use of partial readout acquisitions. By acquiring an asymmetric readout, we have been able to reduce the TR by 20–30%, which is a significant decrease in TR, reducing banding artifacts substantially. This approach has the added benefits of improving the speed performance of the acquisition and reducing velocity artifacts by reducing the first moment of the readout gradient. This approach does require the use of homodyne reconstruction to reconstruct full resolution images, although this is a standard feature on most scanners. Partial readouts also affect the relative phase behavior of water and fat signals as discussed below.

The second approach is to reduce the field inhomogeneity across the heart. Most vendors now offer capabilities for local shimming and second order shimming of the static field to minimize these artifacts by reducing the variations of the off-resonance phase across the selected region to less than 180°. Schar et al. [10] suggested higher order local shimming procedures to avoid bands. An interesting alternative is the use of scout scans acquired with varying center frequencies to identify the center frequency that minimizes the presence of the dark band in the cardiac structures of interest [18]. Short TRs and an improved B_0 homogeneity are also essential to reduce flow induced artifacts in bSSFP imaging [44].

While imaging at 1.5 T does allow for a free choice of the flip angle, the SAR limitations discussed above reduce the maximum achievable flip angle at 3.0 T. Fig. 4 shows a comparison of images acquired at 1.5 T with a flip angle of 60° and acquired at 3.0 T with the highest achievable flip angle of 45° on our scanner. Methods described in Section 2.6 can be used to partially overcome these issues.

Reports in the literature that compare CINE imaging between field strengths with SPGR and bSSFP sequences vary significantly in the reported gains of SNR and CNR [22,45–48]. This might be partly explained by the variability in experimental setup (e.g. coils and sequence parameters such as TR and maximum flip angle). However, in general there is a gain in SNR and CNR with bSSFP compared to SPGR and with imaging at 3.0 T compared to 1.5 T. Several studies document the use of parallel MRI in cardiac CINE imaging with good correlation of volume measurements when using reduction factors of two for a four channel phased-array receiver coil [22,27] and reduction factors of 4 [49] and 6 [29] for 32 element coils. It has been shown that parallel imaging at 3.0 T introduces less SNR degradations than at 1.5 T [27], that the increase in baseline SNR for 3.0 T imaging

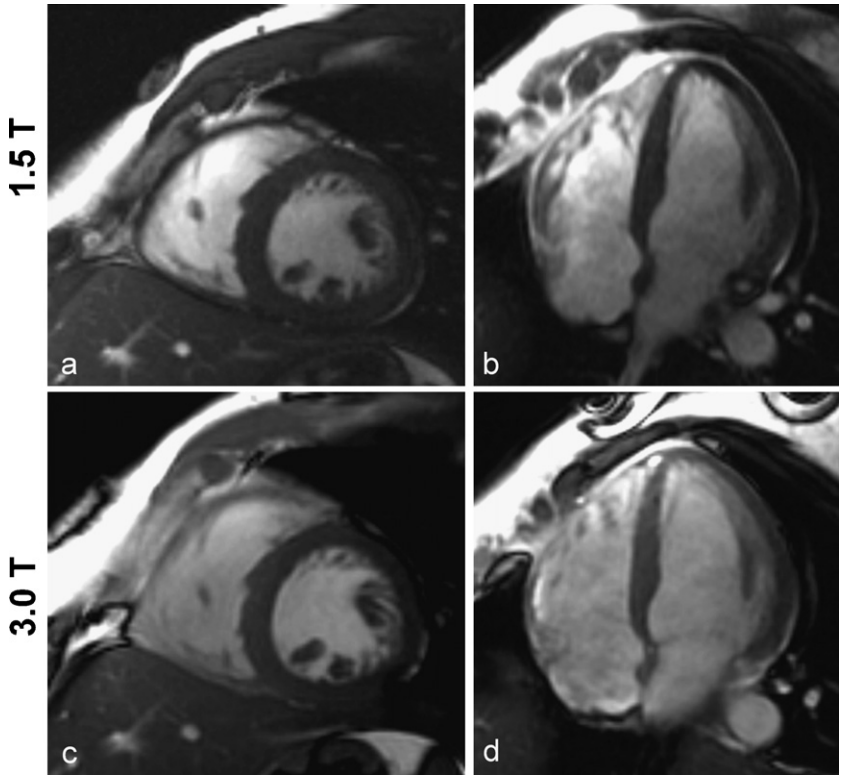

Fig. 4. Cardiac bSSFP acquired at 1.5 T and 3.0 T with identical imaging parameters except of the flip angle of 60° (1.5 T) and 45° (3.0 T). The images were acquired in a short axis view (left column) and four chamber view (right column).

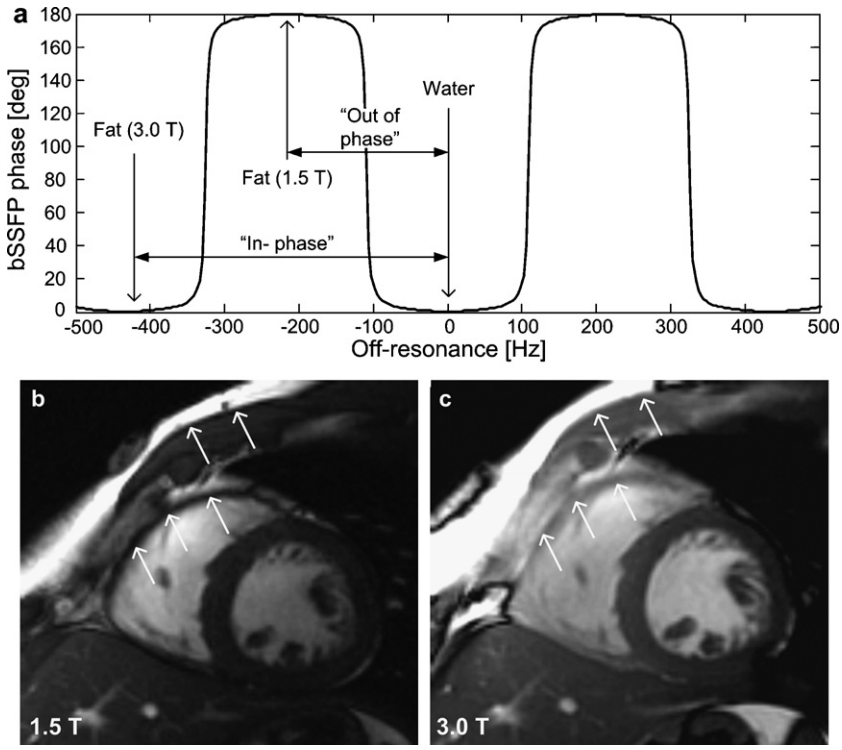

Fig. 5. India-Ink artifacts shown for a volunteer imaged at 1.5 T and 3.0 T with a TR of 4.6 ms. The phase of the bSSFP signal alternates from 0 to 180° between alternating passbands (a). The chemical shift between water and fat at 1.5 T can lead to destructive interference (arrows) in pixels that contain both water and fat (b). That chemical shifts doubles at 3.0 T and leads to changes in the appearance of the water–fat interface. In the absence of field inhomogeneities, the phase of water and fat are identical and signal from water and fat add constructively and the India-Ink artifact disappears (c).

overcompensated for the SNR reduction from parallel imaging [27,49], and that there is good agreement for the measurement of ejection fraction [49]. These gains in acquisition speed cannot only be used to improve spatial or temporal resolution or coverage or reduce a breath-hold duration, it can also decrease the SAR because of a reduced imaging time [34].

3.3. India-Ink artifact with bSSFP

As shown in Fig. 5(b), cardiac SSFP images acquired at 1.5 T are well known to have a black line, or "India-Ink" artifact that occurs at the interfaces of tissues that are predominantly water and predominantly fat. In the heart, this is commonly seen at the border of the pericardium with epicardial fat. This appearance is not a result of chemical shift artifact, which is very small with SSFP because of the high readout bandwidth that is typically used, but rather from the phase behavior of SSFP [50,51]. To explain this appearance, Fig. 5(a) plots the phase behavior of the bSSFP signal using a 60° flip angle, relaxation parameters typical for myocardium at 1.5 T ($T_1 = 800$ ms, $T_2 = 60$ ms), and with TR = 4.6 ms and TE = TR/2 = 2.3 ms. From this figure, it can be seen that the phase behavior of bSSFP alternates from 0 to 180° (π) (i.e., positive to negative) between alternating passbands. This phase behavior always occurs with bSSFP, no matter what the local magnetic field inhomogeneity, so long as TE = TR/2. The chemical shift between water and fat at 1.5 T and 37 °C is −210 Hz, which corresponds exactly to the width of one passband (2π) when TR = 4.6 ms. This means that water and fat signals are always separated by exactly one-pass band, and will always have a 180° (π) phase shift relative to each other. This leads to destructive interference in pixels that contain both water and fat, including those pixels at water–fat interfaces, through partial volume effects. This creates the India-Ink artifact, as is seen with "out of phase" images acquired as part of in/out phase imaging for abdominal imaging [52].

At 3.0 T, the situation changes, however, because the chemical shift between water and fat doubles to −420 Hz, while the gradient performance is roughly the same, and the passband profiles are identical for a given TR. In this situation, however, the water and fat resonances may be separated by two passbands. If the frequency of the passbands is separated by two pass bands, the phase of water and fat are identical and signal from water and fat add constructively, and the India-Ink artifact disappears. Moreover, the presence of field inhomogeneities will cause the resonant peaks of water and fat to shift. Depending on the TR, this may push the resonant peak of fat, for example, into a new passband, before the water moves into a different passband. This complex behavior of the phase can result in changes in the appearance of the water–fat interface, even within the same image, as shown in Fig. 5(c). Although this effect can also occur at 1.5 T (unless the passbands are exactly spaced by 2π, when TR = 4.6 ms), it rarely occurs, because the passbands are relatively wide and the field inhomogeneities are smaller. At 3.0 T, however, the passbands are narrow relative to the chemical shift and field inhomogeneities, and transitions of the water and fat peaks between different passbands frequently occur, as shown

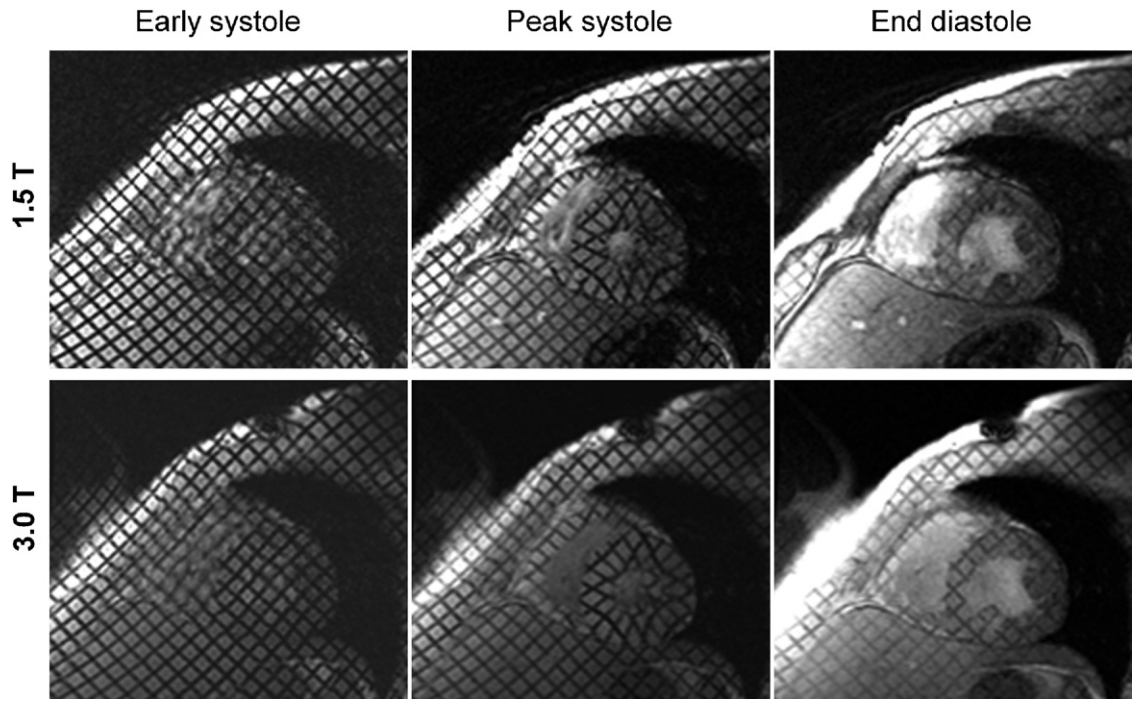

Fig. 6. MR tagging results for a healthy volunteer acquired at 1.5 T (top row) and 3 T (bottom row). Due to the prolonged T_1 relaxation time of the myocardium, the tags persist much longer as evident in the end diastolic image shown in the right column.

in Fig. 5(a). The importance of understanding this artifact is to understand differences in appearance between 1.5 T and 3.0 T, and to avoid pitfalls that can result from relying on the presence of this artifact (e.g. using the India-Ink artifact to identify fatty masses such as lipomas).

Finally, it is important to note that the phase behavior shown in Fig. 2(b) and Fig. 5(a) occurs only when TE = TR/2, the most commonly used TE for symmetric echo acquisitions in SSFP. However, as we have suggested above, the use of partial readout (k_x) acquisitions is a useful way to shorten the TR at 3.0 T to reduce banding and flow artifacts. For echo times not equal to TR/2, the phase behavior is more complex and will lead to more complex interference of water and fat at tissue interfaces. While the appearance is not disruptive to image interpretation, it is important to note this phase behavior to avoid diagnostic pitfalls regarding fatty tissue at tissue interface, i.e., the interpretating physician should not rely on the presence of the India-Ink artifact, particularly at 3.0 T.

4. MR tagging

MR tagging allows for the evaluation of complex intramyocardial contractile patterns and quantitative motion analysis of the cardiac walls [53,54]. With this method, intrinsic markers in the myocardial wall are created by the application of inversion bands across the imaging plane. This pattern is accomplished by the use of RF pulses in combination with gradient pulses that invert spins in thin parallel planes perpendicular to the imaging plane just prior to the application of the RF pulse used for the excitation of the imaging plane. Radial, line, and grid-shaped patterns [55] have been applied to track the evolution of these bands throughout the cardiac cycle for the assessment of the deformation of the myocardium and e.g. identify regions of impaired contractility. Spoiled gradient echo CINE sequences as described above for functional imaging are usually used for MR tagging with the simple addition of the saturation pulses. One challenge encountered with tagging at 1.5 T is the fading of tags at end-diastole, greatly limiting the evaluation of myocardial function during diastole. Although MR tagging at 3.0 T benefits from the increased SNR and CNR, the most important benefit is the prolonged T_1 of myocardium. This leads to a slower recovery of the longitudinal magnetization and, therefore, improved tag persistence, particularly in mid- and end-diastole, where tags have typically faded when imaging at 1.5 T. This effect is shown in Fig. 6, where a healthy volunteer was imaged in a short axis view with a grid tag pattern. While the tags can be seen well at both field strengths during early and late systole, the images acquired during late diastole show faded tags at 1.5 T while the contrast at 3.0 T is still sufficient for a good delineation of the tags. A recent study [56] showed SNR improvements of 35% and CNR improvements of 80% for myocardial tags at 3.0 T as compared to 1.5 T. Gutberlet et al. [27] measured gains in SNR and CNR during systole as 54% and 174%, respectively. Fig. 7 shows a clinical example of hypertrophic cardiomyopathy (HCM) with abnormally decreased myocardial contraction in the anteroseptal wall of the left ventricle (long arrows) in the tagged end-systolic image.

5. First pass perfusion imaging

Most MR myocardial perfusion acquisitions measure signal changes in the myocardial wall during the first pass

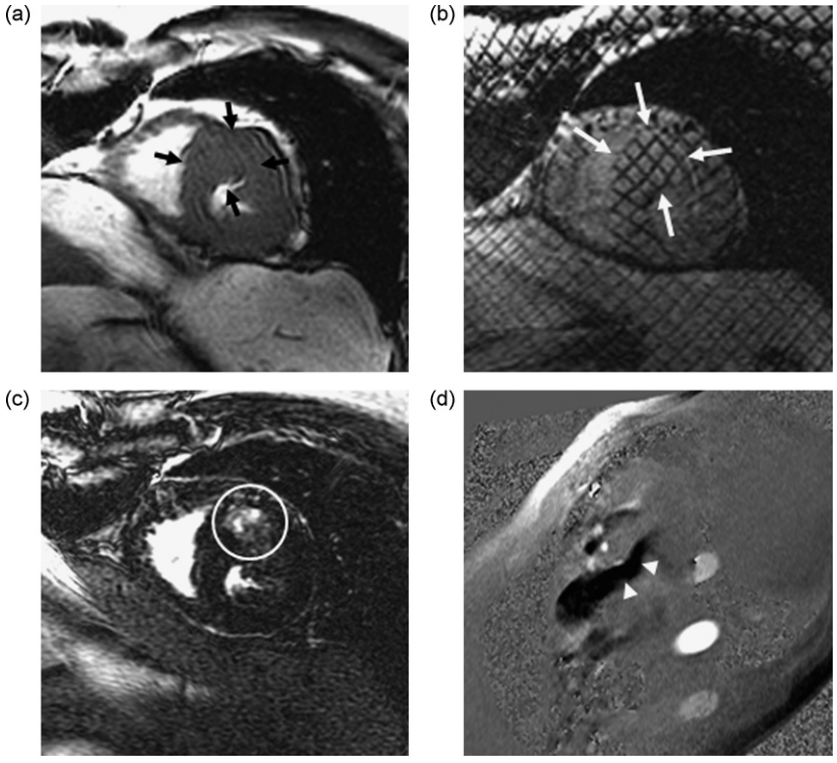

Fig. 7. Sixty-five-year old man with hypertrophic cardiomyopathy (HCM). Short-axis bSSFP (a), tagged end-systolic (b), and delayed contrast-enhanced (c) images demonstrate asymmetric thickening (short arrows), abnormally decreased myocardial contraction (long arrows), and patchy mid-myocardial enhancement (circle) in the anteroseptal and anterolateral walls of the left ventricle, respectively. Left ventricular outflow tract view (three-chamber) in-plane phase contrast image (d) reveals sub-valvular flow acceleration (arrowheads) characteristic of HCM.

of a Gadolinium-based contrast bolus into the coronary bed [57]. While the extracellular contrast agent leaks into the myocardium, it shortens its T_1. This signal change can be observed with rapid, dynamic T_1 weighted imaging sequences to detect hypointense regions with perfusion defects. Although visual inspection of the data is the most commonly used approach, parameters related to myocardial perfusion can also be measured in a semiquantitatively or quantitatively fashion [58]. The in-plane resolution of MR perfusion imaging (2–3 mm) surpasses the spatial resolution of positron emission tomography (PET) and single-photon emission photography (SPECT) perfusion imaging and allows for the separation of defects in the endo- and epicardial wall. In some studies, patients are pharmaceutically stressed with vasodilators to measure the perfusion under maximum flow or to assess myocardial flow reserve. Despite large improvements in scanner hardware and sequence design since its initial conception [59,60], the demands on myocardial perfusion MR remain high and leave room for improvement. Ideally, the acquisition provides (1) high spatial (<3 mm) and (2) temporal (every RR interval) resolution, (3) whole heart coverage, (4) a quantifiable relationship between signal intensity and contrast agent concentration to allow for quantification, and (5) good image quality with sufficiently high CNR [61].

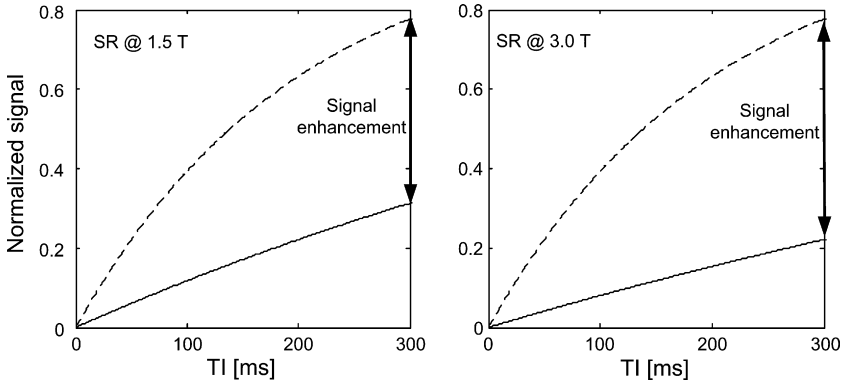

Fig. 8. Representative signal curves for MR perfusion measurements at 1.5 T (left column) and 3.0 T (right column) with a saturation recovery sequence. The extracellular contrast agent leaks into the myocardium, shortens its T_1, and generates a similar signal levels (solid lines) at both field strengths. The T_1 lengthening effect of the higher field strength leads to an increased signal difference for the hypoperfused regions (dashed lines).

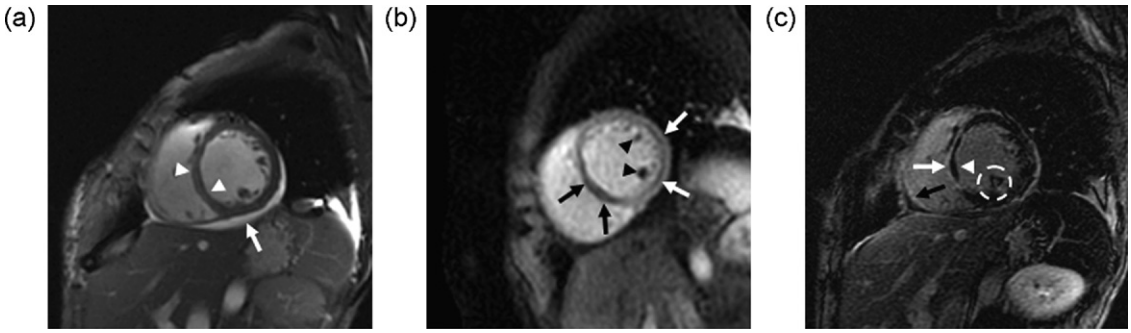

Fig. 9. Twenty-nine-year old woman with Churg-Strauss syndrome (allergic angiitis and granulomatosis) and endomyocardial biopsy proven eosinophilic myocarditis. At time of cardiac MRI, patient presented with shortness of breath and chest pain. Laboratory evaluations revealed elevated serum troponin levels and abnormal electrocardiogram. Short-axis bSSFP image (a) reveals a small pericardial effusion (arrow) and mild thinning and hyperintensity in the interventricular septum (arrowheads). Left ventricular ejection fraction calculated from cine bSSFP images was 33%. First-pass resting perfusion imaging (b) demonstrates transmural hypoperfusion in the interventricular septum (black arrows), subendocardial hypoperfusion in the lateral wall (white arrows) and hypoperfusion of the papillary muscles (arrowheads). Delayed contrast-enhanced viability images (c) show transmural enhancement in the interventricular septum (white arrow) with an area of hypoenhancement (arrowhead) indicating microvascular obstruction, or "no-reflow." The posterior papillary muscle (dashed circle) and right ventricular free wall (black arrow) also have abnormal delayed contrast-enhancement.

While various approaches for perfusion imaging exist, the most commonly used sequence is based on a 2D multislice, spoiled gradient echo sequence with saturation recovery (SR) preparation. The saturation pulse is applied prior to the readout for each acquired slice. The duration between the application of the saturation pulse and the acquisition of the contrast defining central *k*-space lines, known as "TI", similar to the inversion time in inversion recovery sequences even though this is not an inversion pulse. As shown in Fig. 8, the signal difference between normal myocardium and regions with perfusion deficits is based on the differences in the T_1 and the chosen TI. MR perfusion imaging at 3.0 T benefits from the increased SNR and CNR but also from the T_1 lengthening of the myocardium in the hypoperfused region. In this way, an additional improvement in contrast between normal and hypoperfused myocardium can be achieved, beyond the factor of two increase from SNR improvements alone. As shown in Fig. 8, the signal recovery of the normally perfused region is similar between 1.5 T and 3.0 T because of the presence of the Gd-based contrast agent while the rate of signal recovery of underperfused areas is reduced, resulting in an increased contrast between perfused and hypoperfused myocardium, as compared to 1.5 T. These theoretical predictions are supported by clinical results with significant image improvements and diagnostic performance [62] at 3.0 T. Gutberlet et al. [22] measured an increase in SNR of 109% and in CNR between myocardium and the left ventricular cavity of 87% while Araoz et al. [63] measured an increase in contrast enhancement ratio of 70% and in myocardial enhancement ratio of 291%. The increased CNR allows for an improved detection of small perfusion defects. Fig. 9 is a clinical example of abnormal perfusion in a patient with Churg-Strauss syndrome (eosinophilic myocarditis). The image reveals transmural hypoperfusion in the interventricular septum (black arrows), subendocardial hypoperfusion in the lateral wall (white arrows) and hypoperfusion of the papillary muscles (arrowheads).

MR perfusion imaging at 3.0 T can also benefit significantly from the use of parallel imaging with higher acceleration factors in order to improve temporal and spatial resolution of the acquisition, as well as increasing coverage over the entire heart. Optimal injection protocols should be determined for given sequences and modes of analysis to balance the optimization of contrast and minimization of contrast-induced susceptiblity artifacts [64].

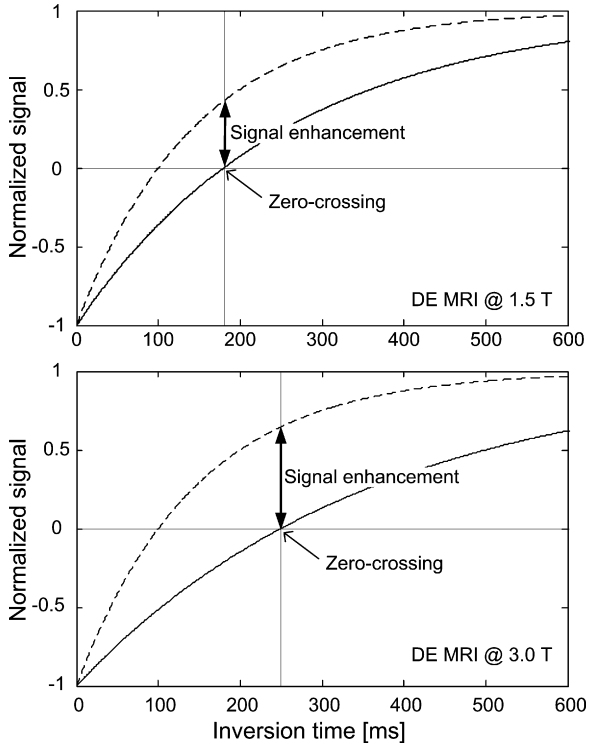

Fig. 10. Representative signal curves for delayed enhancement measurements at 1.5 T (top row) and 3 T (bottom row). The TI time for imaging is chosen such that the signal from normal myocardium (dashed line) is "nulled". While the recovery of the signal for infarcted myocardium remains similar (solid line), the T_1 lengthening of the normal myocardium leads to an increased signal enhancement at 3.0 T.

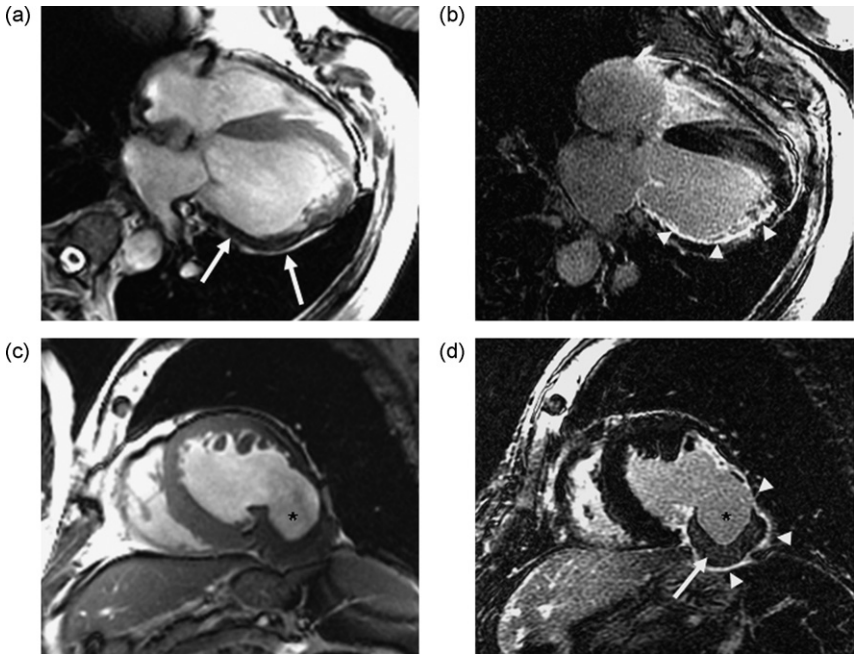

Fig. 11. Sixty-nine-year old man with old left lateral and inferolateral wall myocardial infarction. Horizontal long axis bSSFP image (a) demonstrates a thin, hypointense lateral wall (arrows). Delayed contrast-enhanced image (d) confirms subendocardial enhancement in the lateral wall from base to apex (arrowheads). Short axis bSSFP (c) and delayed contrast-enhanced (d) images reveal a pseudoaneurysm (asterisk) arising from the inferolateral wall of the basal left ventricle. The delayed contrast-enhanced image shows transmural enhancement (arrowheads) with a large thrombus (arrow) in the pseudoaneurysm.

6. Viability imaging—delayed enhancement

Evaluation of myocardial infarction using delayed imaging after intravenous injection of Gadolinium based contrast agents has become the gold standard for the evaluation of myocardial viability [4]. Areas of infarcted myocardium (acute or chronic) retain gadolinium for prolonged periods, and delayed imaging at approximately 10–20 min after the intra-venous injection, when the concentration of Gadolinium in normal myocardium has washed out, provides an opportunity for visualizing areas of infarction with very high conspicuity. It is important to note, that slower clearance of the contrast agent cannot only occur in scars but also in a variety of other disorders such as inflammatory or infectious diseases of the myocardium, cardiomyopathy, cardiac neoplasms, and congenital or genetic cardiac pathologic conditions [65], and therefore delayed enhancement is relatively non-specific.

Delayed enhancement (DE) can be visualized with a variety of cardiac gated T_1 weighted imaging sequences, but most practitioners use the inversion-recovery spoiled gradient echo (IR-SPGR) method first described by Simonetti et al. [66]. In this approach, T_1 weighting is achieved by applying a non-selective inversion pulse and waiting an inversion time (TI) until the normal myocardium has "nulled", i.e., zero longitudinal magnetization. At this time a rapid, segmented SPGR acquisition acquires several lines of *k*-space, and this approach is repeated over several heartbeats until the acquisition is complete. By choosing a TI time that nulls the normal myocardium, areas of enhancing tissue appear very conspicuous and are easily visualized. This principle is visualized in Fig. 10.

To null the myocardium, the clinician must choose the correct TI time, which depends on the T_1 of the normal myocardium. This value is influenced by the amount of gadolinium in the blood, which is determined by the initial dose given, the time from that dose and the clearance of gadolinium from the blood. Clearance of contrast from blood depends on the patient's cardiac output and renal function. The T_1 of the myocardium is also dependent on the field strength of the magnet. The maximum signal difference between normal and enhanced myocardium actually occurs later than the zero crossing of the signal intensity of the normal myocardium, but the conspicuity of lesions is the highest at this point. As discussed above, the T_1 of myocardium increases considerably, meaning that the inversion time needed to null the myocardium will increase from values typically used at 1.5 T. In our experience, the TI increases from 180–200 ms at 1.5 T to approximately 220–250 ms at 3.0 T. The patient specific optimal TI is determined by trial and error or advanced scout scans [67] that rapidly generate images with multiple TIs at a lower quality to identify the optimal timing.

Delayed enhancement imaging benefits from a higher magnetic field in several ways. In addition to the increase in SNR and CNR from the higher magnetization, the increase in T_1 of the normal myocardium also leads to increased difference in the signal between normal and enhancing myocardium. This occurs because the normal myocardium recovers more slowly, requiring a long TI, that leads to an increase in the absolute signal difference between normal and enhancing myocardium. An example of this improved CNR is shown in Fig. 10. Recent studies have demonstrated significant improvements in image quality, SNR and CNR for DE MRI at 3.0 T over 1.5 T [22,68].

The improved CNR supports an improved delineation of infarct extend. Figs. 7, 9 and 11 show various clinical examples of delayed enhancement images acquired with a slice thickness as small as 6 mm (Fig. 11).

Proper signal nulling with the inversion recovery sequence requires a homogeneous 180° flip angle across the imaging slice. The decreased B_1 homogeneity at 3.0 T causes larger deviations from the ideal flip angle and, therefore, signal nulling of the myocardium might not be achieved uniformly across the heart. The use of adiabatic pulses can provide a more homogeneous flip angle to avoid this undesired effect [22]. These pulses are designed to sweep the resonant frequency and amplitude of the RF pulse to drive magnetization in a manner that is insensitive to the actual B_1.

The phase sensitive inversion recovery (PSIR) sequence [69] provides delayed enhancement images with more stable contrast even if a suboptimal TI was chosen. This sequence has also been successfully applied on 3.0 T systems [70].

7. Conclusion

In conclusion, the most important benefits of cardiac imaging at 3.0 T arise from the increased SNR and CNR and the longer longitudinal relaxation time T_1. The latter leads to an improved background suppression and improved contrast and superior detection of small defects in first pass perfusion imaging and an improved delineation of infarct extent in viability imaging. The increased SNR and benefits of 3.0 T for parallel imaging can be used for accelerated imaging to provide more coverage or higher spatial or temporal resolution. The biggest challenges for cardiac imaging at a higher field strength are SAR limitations and the decreased B_1 homogeneity and increased susceptibility effects. These issues can be partly overcome by advanced sequence design, adiabatic pulses, and improved shimming techniques.

While the gains of a higher field strength are somewhat offset by the presence of more severe artifacts for CINE imaging with bSSFP, almost all other cardiac sequences including MR tagging, myocardial perfusion and delayed enhancement imaging clearly benefit from the higher field strength. With proper shimming, and attention to methods to maintain a short TR, it is relatively straightforward to acquire highly diagnostic bSSFP images in all patients.

Other important CMR applications not discussed in this manuscript including coronary artery imaging [11,71,72] and phase contrast imaging [22] (see also Fig. 7) have also been successfully adopted to clinical 3.0 T imaging. Particularly the combination of parallel MRI with multi-element coils and high acceleration factors offers unique opportunities for improved cardiovascular MRI.

In summary, cardiac imaging at 3.0 T offers tremendous advantages beyond the increase in SNR performance, including improved contrast enhanced perfusion and viability imaging, improved opportunities for aggressive parallel imaging techniques, and improved visualization of wall motion through myocardial tagging. Advancements in localized shimming methods and new RF pulses to reduce SAR to avoid pitfalls from B1 inhomogeneities will complete the transformation of 3.0 T cardiac imaging from vision to a clinical reality in daily practice.

References

[1] A. H. A. (AHA), "Heart Disease and Stroke Statistics – 2007 Update At-a-Glance," American Heart Association 2006.
[2] Cannon CP, Braunwald E, McCabe CH, et al. Intensive versus moderate lipid lowering with statins after acute coronary syndromes. N Engl J Med 2004;350:1495–504.
[3] Sakuma H. Magnetic resonance imaging for ischemic heart disease. J Magn Reson Imaging 2007;26:3–13.
[4] Kim RJ, Wu E, Rafael A, et al. The use of contrast-enhanced magnetic resonance imaging to identify reversible myocardial dysfunction. N Engl J Med 2000;343:1445–53.
[5] Haacke EM, Brown RB, Thompson MR, Venekatesan R. Magnetic resonance imaging—principals and sequence design. New York, NY: John Wiley & Sons; 1999.
[6] Fenchel M, Kramer U, Nael K, Miller S. Cardiac magnetic resonance imaging at 3.0 T. Top Magn Reson Imaging 2007;18:95–104.
[7] Bottomley PA, Foster TH, Argersinger RE, Pfeifer LM. A review of normal tissue hydrogen NMR relaxation times and relaxation mechanisms from 1–100 MHz: dependence on tissue type, NMR frequency, temperature, species, excision, and age. Med Phys 1984;11:425–48.
[8] Stanisz GJ, Li JG, Wright GA, Henkelman RM. Water dynamics in human blood via combined measurements of T2 relaxation and diffusion in the presence of gadolinium. Magn Reson Med 1998;39:223–33.
[9] Noeske R, Seifert F, Rhein KH, Rinneberg H. Human cardiac imaging at 3 T using phased array coils. Magn Reson Med 2000;44:978–82.
[10] Schar M, Kozerke S, Fischer SE, Boesiger P. Cardiac SSFP imaging at 3 Tesla. Magn Reson Med 2004;51:799–806.
[11] Bi X, Deshpande V, Simonetti O, Laub G, Li D. Three-dimensional breath-hold SSFP coronary MRA: a comparison between 1.5 T and 3.0 T. J Magn Reson Imaging 2005;22:206–12.
[12] Stanisz GJ, Odrobina EE, Pun J, et al. T1, T2 relaxation and magnetization transfer in tissue at 3 T. Magn Reson Med 2005;54:507–12.
[13] Sharma P, Socolow J, Patel S, Pettigrew RI, Oshinski JN. Effect of Gd-DTPA-BMA on blood and myocardial T1 at 1.5 T and 3 T in humans. J Magn Reson Imaging 2006;23:323–30.
[14] Rohrer M, Bauer H, Mintorovitch J, Requardt M, Weinmann HJ. Comparison of magnetic properties of MRI contrast media solutions at different magnetic field strengths. Invest Radiol 2005;40:715–24.
[15] Pintaske J, Martirosian P, Graf H, et al. Relaxivity of gadopentetate dimeglumine (magnevist), gadobutrol (gadovist), and gadobenate dimeglumine (MultiHance) in human blood plasma at 0.2, 1.5, and 3 Tesla. Invest Radiol 2006;41:213–21.
[16] Neubauer S. Cardiac magnetic resonance spectroscopy. Curr Cardiol Rep 2003;5:75–82.
[17] Atalay MK, Poncelet BP, Kantor HL, Brady TJ, Weisskoff RM. Cardiac susceptibility artifacts arising from the heart-lung interface. Magn Reson Med 2001;45:341–5.
[18] Deshpande VS, Shea SM, Li D. Artifact reduction in true-FISP imaging of the coronary arteries by adjusting imaging frequency. Magn Reson Med 2003;49:803–9.
[19] Hargreaves BA, Cunningham CH, Nishimura DG, Conolly SM. Variable-rate selective excitation for rapid MRI sequences. Magn Reson Med 2004;52:590–7.
[20] Busse RF. Reduced RF power without blurring: correcting for modulation of refocusing flip angle in FSE sequences. Magn Reson Med 2004;51:1031–7.
[21] Hennig J, Weigel M, Scheffler K. Multiecho sequences with variable refocusing flip angles: optimization of signal behavior using smooth transitions between pseudo steady states (TRAPS). Magn Reson Med 2003;49:527–35.

[22] Gutberlet M, Noeske R, Schwinge K, Freyhardt P, Felix R, Niendorf T. Comprehensive cardiac magnetic resonance imaging at 3.0 Tesla: feasibility and implications for clinical applications. Invest Radiol 2006;41:154–67.
[23] Nezafat R, Stuber M, Ouwerkerk R, Gharib AM, Desai MY, Pettigrew RI. B1-insensitive T_2 preparation for improved coronary magnetic resonance angiography at 3 T. Magn Reson Med 2006;55:858–64.
[24] Sodickson DK, Manning WJ. Simultaneous acquisition of spatial harmonics (SMASH): fast imaging with radiofrequency coil arrays. Magn Reson Med 1997;38:591–603.
[25] Pruessmann KP, Weiger M, Scheidegger MB, Boesiger P. SENSE: sensitivity encoding for fast MRI. Magn Reson Med 1999;42: 952–62.
[26] Griswold MA, Jakob PM, Heidemann RM, et al. Generalized autocalibrating partially parallel acquisitions (GRAPPA). Magn Reson Med 2002;47:1202–10.
[27] Gutberlet M, Schwinge K, Freyhardt P, et al. Influence of high magnetic field strengths and parallel acquisition strategies on image quality in cardiac 2D CINE magnetic resonance imaging: comparison of 1.5 T vs. 3.0 T. Eur Radiol 2005;15:1586–97.
[28] Reeder SB, Wintersperger BJ, Dietrich O, et al. Practical approaches to the evaluation of signal-to-noise ratio performance with parallel imaging: application with cardiac imaging and a 32-channel cardiac coil. Magn Reson Med 2005;54:748–54.
[29] Fenchel M, Deshpande VS, Nael K, et al. Cardiac cine imaging at 3 Tesla: initial experience with a 32-element body-array coil. Invest Radiol 2006;41:601–8.
[30] Hardy CJ, Cline HE, Giaquinto RO, Niendorf T, Grant AK, Sodickson DK. 32-Element receiver-coil array for cardiac imaging. Magn Reson Med 2006;55:1142–9.
[31] Wintersperger BJ, Reeder SB, Nikolaou K, et al. Cardiac CINE MR imaging with a 32-channel cardiac coil and parallel imaging: impact of acceleration factors on image quality and volumetric accuracy. J Magn Reson Imaging 2006;23:222–7.
[32] Ohliger MA, Grant AK, Sodickson DK. Ultimate intrinsic signal-to-noise ratio for parallel MRI: electromagnetic field considerations. Magn Reson Med 2003;50:1018–30.
[33] Wiesinger F, Van de Moortele PF, Adriany G, De Zanche N, Ugurbil K, Pruessmann KP. Parallel imaging performance as a function of field strength—an experimental investigation using electrodynamic scaling. Magn Reson Med 2004;52:953–64.
[34] Niendorf T, Sodickson DK. Highly accelerated cardiovascular MR imaging using many channel technology: concepts and clinical applications. Eur Radiol 2007.
[35] Atkinson DJ, Edelman RR. Cineangiography of the heart in a single breath hold with a segmented turboFLASH sequence. Radiology 1991;178:357–60.
[36] Haase A, Frahm J, Matthaei D, Hanicke W, Merboldt KD. Flash imaging—rapid Nmr imaging using low flip-angle pulses. J Magn Reson 1986;67:258–66.
[37] Carr HY. Steady-state free precession in nuclear magnetic resonance. Phys Rev 1956;112:1693–701.
[38] Oppelt A, Graumann R, Barfus H, Fischer H, Hartl W, Shajor W. FISP-a new fast MRI sequence. Electromedica 1986;54:15–8.
[39] Carr JC, Simonetti O, Bundy J, Li D, Pereles S, Finn JP. Cine MR angiography of the heart with segmented true fast imaging with steady-state precession. Radiology 2001;219:828–34.
[40] Moon JC, Lorenz CH, Francis JM, Smith GC, Pennell DJ. Breath-hold FLASH and FISP cardiovascular MR imaging: left ventricular volume differences and reproducibility. Radiology 2002;223: 789–97.
[41] Plein S, Bloomer TN, Ridgway JP, Jones TR, Bainbridge GJ, Sivananthan MU. Steady-state free precession magnetic resonance imaging of the heart: comparison with segmented *k*-space gradient-echo imaging. J Magn Reson Imaging 2001;14:230–6.
[42] Sekihara K. Steady-state magnetizations in rapid NMR imaging using small flip angles and short repetition intervals. IEEE Trans Med Imaging 1987;6:157–64.
[43] Zur Y, Stokar S, Bendel P. An analysis of fast imaging sequences with steady-state transverse magnetization refocusing. Magn Reson Med 1988;6:175–93.
[44] Markl M, Pelc NJ. On flow effects in balanced steady-state free precession imaging: pictorial description, parameter dependence, and clinical implications. J Magn Reson Imaging 2004;20:697–705.
[45] Hinton DP, Wald LL, Pitts J, Schmitt F. Comparison of cardiac MRI on 1.5 and 3.0 Tesla clinical whole body systems. Invest Radiol 2003;38: 436–42.
[46] Hudsmith LE, Petersen SE, Tyler DJ, et al. Determination of cardiac volumes and mass with FLASH and SSFP cine sequences at 1.5 vs. 3 Tesla: a validation study. J Magn Reson Imaging 2006;24:312–8.
[47] Michaely HJ, Nael K, Schoenberg SO, et al. Analysis of cardiac function—comparison between 1.5 Tesla and 3.0 Tesla cardiac cine magnetic resonance imaging: preliminary experience. Invest Radiol 2006;41:133–40.
[48] Tyler DJ, Hudsmith LE, Petersen SE, et al. Cardiac cine MR-imaging at 3T: FLASH vs. SSFP. J Cardiovasc Magn Reson 2006;8:709–15.
[49] Wintersperger BJ, Bauner K, Reeder SB, et al. Cardiac steady-state free precession CINE magnetic resonance imaging at 3.0 Tesla: impact of parallel imaging acceleration on volumetric accuracy and signal parameters. Invest Radiol 2006;41:141–7.
[50] Hargreaves BA, Vasanawala SS, Nayak KS, Hu BS, Nishimura DG. Fat-suppressed steady-state free precession imaging using phase detection. Magn Reson Med 2003;50:210–3.
[51] Scheffler K, Hennig J. Is TrueFISP a gradient-echo or a spin-echo sequence? Magn Reson Med 2003;49:395–7.
[52] Dixon WT. Simple proton spectroscopic imaging. Radiology 1984;153:189–94.
[53] McVeigh ER. MRI of myocardial function: motion tracking techniques. Magn Reson Imaging 1996;14:137–50.
[54] Zerhouni EA, Parish DM, Rogers WJ, Yang A, Shapiro EP. Human heart: tagging with MR imaging—a method for noninvasive assessment of myocardial motion. Radiology 1988;169:59–63.
[55] Rademakers FE. Left ventricular myocardial tagging. In: Nagel E, van Rossum AC, Fleck E, editors. Cardiovascular magnetic resonance. Darmstad, Germany: Steinkopff; 2004. p. 302.
[56] Kramer U, Deshpande V, Fenchel M, et al. Cardiac MR tagging: optimization of sequence parameters and comparison at 1.5 T and 3.0 T in a volunteer study. Rofo 2006;178:515–24.
[57] Gebker R, Schwitter J, Fleck E, Nagel E. How we perform myocardial perfusion with cardiovascular magnetic resonance. J Cardiovasc Magn Reson 2007;9:539–47.
[58] Crean A, Merchant N. MR perfusion and delayed enhancement imaging in the heart. Clin Radiol 2006;61:225–36.
[59] Atkinson DJ, Burstein D, Edelman RR. First-pass cardiac perfusion: evaluation with ultrafast MR imaging. Radiology 1990;174:757–62.
[60] McNamara MT, Higgins CB, Ehman RL, Revel D, Sievers R, Brasch RC. Acute myocardial ischemia: magnetic resonance contrast enhancement with gadolinium-DTPA. Radiology 1984;153:157–63.
[61] Kellman P, Arai AE. Imaging sequences for first pass perfusion—a review. J Cardiovasc Magn Reson 2007;9:525–37.
[62] Cheng AS, Pegg TJ, Karamitsos TD, et al. Cardiovascular magnetic resonance perfusion imaging at 3-Tesla for the detection of coronary artery disease: a comparison with 1.5-Tesla. J Am Coll Cardiol 2007;49: 2440–9.
[63] Araoz PA, Glockner JF, McGee KP, et al. 3 Tesla MR imaging provides improved contrast in first-pass myocardial perfusion imaging over a range of gadolinium doses. J Cardiovasc Magn Reson 2005;7:559–64.
[64] Su MY, Yang KC, Wu CC, et al. First-pass myocardial perfusion cardiovascular magnetic resonance at 3 Tesla. J Cardiovasc Magn Reson 2007;9:633–44.
[65] Vogel-Claussen J, Rochitte CE, Wu KC, et al. Delayed enhancement MR imaging: utility in myocardial assessment. Radiographics 2006;26:795–810.
[66] Simonetti OP, Kim RJ, Fieno DS, et al. An improved MR imaging technique for the visualization of myocardial infarction. Radiology 2001;218: 215–23.

[67] Huber AM, Schoenberg SO, Hayes C, et al. Phase-sensitive inversion-recovery MR imaging in the detection of myocardial infarction. Radiology 2005;237:854–60.

[68] Klumpp B, Fenchel M, Hoevelborn T, et al. Assessment of myocardial viability using delayed enhancement magnetic resonance imaging at 3.0 Tesla. Invest Radiol 2006;41:661–7.

[69] Kellman P, Arai AE, McVeigh ER, Aletras AH. Phase-sensitive inversion recovery for detecting myocardial infarction using gadolinium-delayed hyperenhancement. Magn Reson Med 2002;47:372–83.

[70] Huber A, Bauner K, Wintersperger BJ, et al. Phase-sensitive inversion recovery (PSIR) single-shot TrueFISP for assessment of myocardial infarction at 3 Tesla. Invest Radiol 2006;41:148–53.

[71] Huber ME, Kozerke S, Pruessmann KP, Smink J, Boesiger P. Sensitivity-encoded coronary MRA at 3 T. Magn Reson Med 2004;52: 221–7.

[72] Gharib AM, Herzka DA, Ustun AO, et al. Coronary MR angiography at 3 T during diastole and systole. J Magn Reson Imaging 2007;26: 921–6.